Synthesis and characterisation of flame-sprayed superparamagnetic bare and silica-coated maghemite nanoparticles

Wey Yang Teoh[*], Dan Li[*], Cordelia Selomulya[**] , Robert Woodward[***], and Rose Amal[*]

[*]ARC Centre for Functional Nanomaterials, School of Chemical Sciences and Engineering, The University of New South Wales, Sydney, NSW 2052, AUSTRALIA
[**]Department of Chemical Engineering, Clayton campus, Monash University, VIC 3800, AUSTRALIA
[***]Nanomagnetics and Spin Dynamics Group, School of Physics, University of Western Australia, Crawley, WA 6009, AUSTRALIA

ABSTRACT

Flame Spray Pyrolysis (FSP) was used to synthesize γ-Fe_2O_3 and SiO_2/γ-Fe_2O_3 nanoparticles of different sizes (d_{BET} = 5-60 nm). Bare γ-Fe_2O_3 displays unique hexagonal/octagonal disc-shaped nanoparticles, while different morphology of SiO_2/γ-Fe_2O_3 nanoparticles could be produced by varying the ratio of silica and iron precursors during synthesis. The particles were predominantly superparamagnetic at room temperature. The understanding on how different nanostructures were formed was obtained through characterisation of their properties using Transmission Electron Microscopy, X-ray Diffraction, Atomic Force Microscopy, N_2 adsorption, and Superconducting Quantum Interference Device magnetometer. The study is particularly useful in order to tailor the properties of these magnetic nanoparticles during synthesis for bio-related applications.

Keywords: flame spray pyrolysis, maghemite nanoparticles, synthesis, characterisation

1 INTRODUCTION

Magnetic nanoparticles possess physiochemical, magnetic, and optical properties that are of great importance in a variety of bio-applications, including selective protein separation and digestion, High Gradient Magnetic Fishing, drug carrier, MRI contrast agent and cell-tracking, cancer therapy, and DNA analysis. The desired properties include high saturation magnetisation and coercivity, high stability, and bio-compatible surface properties [1]. Another unique property is superparamagnetism, which causes the particles to behave like magnetic entities only in the presence of external magnetic field. This particular characteristic is desirable as it helps avoid magnetically-induced self aggregation that could alter the functionality of the system, as well as allowing the particles to be manipulated for targeted flow. It is usually observed at size below 20nm for magnetite and maghemite particles at room temperature. However, depending on the synthesis methods, particles at that size level often have poor crystallinity and magnetic strength. It is therefore important to understand how these particles are formed at the atomic level and how the formation mechanisms influence the particle properties.

In this work, a single phase γ-Fe_2O_3 and mixed phases SiO_2/γ-Fe_2O_3 nanoparticles were formed via liquid-fed Flame Spray Pyrolysis (FSP) in a one-step process. Various techniques such as Transmission Electron Microscopy (TEM), X-Ray Diffraction (XRD), Atomic Force Microscopy (AFM) and Superconducting Quantum Interference Device (SQUID) magnetometer were used to characterize the physiochemical, micro-structural, and magnetic properties of these particles. The detailed study helps to understand the crystal growth mechanisms within the flame, which serves as a well-defined platform both for comparison with other synthesis techniques and for tailoring the particle properties for specific applications.

2 EXPERIMENTS

2.1 Synthesis

Iron (III) acetylacetonate ($Fe(acac)_3$, Aldrich, 97%) was dissolved in a xylene (Riedel-de-Haen, analytical grade) / acetonitrile (JT Baker, HPLC grade) mixture (volume ratio 63/22) to a final concentration of 0.32 M. The combustion enthalpy of this mixture used as the precursor for γ-Fe_2O_3 synthesis was -26.7 kJ / ml. Tetraethyl orthosilicate (TEOS, Aldrich, 98%) was added for the synthesis of SiO_2/γ-Fe_2O_3 according to the desired Fe:Si ratio while maintaining the $Fe(acac)_3$ concentration at 0.32 M. The xylene/acetonitrile ratio was adjusted to match the combustion enthalpy of Fe-only precursor. For the synthesis of γ-Fe_2O_3, the ratios of the liquid precursor feed flowrate (in ml/min) to dispersant O_2 gas flowrate (in L/min) were 1:5, 3:5, 5:5, 7:5, 10:5, and 12:3, respectively. In the synthesis of SiO_2/γ-Fe_2O_3, only the 10:5 ratio was used. The liquid precursor was introduced via a syringe pump (Inotech R233) into the pressure-assisted nozzle (1.5 bar), where atomisation occurred. The fine droplets were combusted by the surrounding methane/oxygen (1.5 L/min / 3.2 L/min) supporting flame forming a self-sustaining main core flame.

An additional 5 L/min of sheath O_2 were provided through an outermost sintered metal ring. The synthesized nanoparticles were collected on a glass fibre filter (Whatmann GF/D, 25.7 cm diameter) with the aid of a vacuum pump (Alcatel SD Series). In the latter experiments, a quartz tube was placed on the nozzle to confine the flame during the synthesis of γ-Fe_2O_3 and SiO_2/γ-Fe_2O_3 at a liquid precursor (ml/min) to dispersant O_2 (L/min) ratio of 8:5.

2.2 Characterisation

X-ray diffraction (Cu Kα radiation scanned for 2θ = 20-70˚ with a step size of 0.02˚ and scan speed of 0.6˚/min) was used to identify the phase of as-prepared powders. The crystallite size (d_{XRD}) of γ-Fe_2O_3 (311) phase was calculated using the Scherrer formula. The morphologies of different samples were observed using Transmission Electron Microscopy (TEM), while size distribution was statistically determined based on minimum 150 particle counts. N_2 adsorption at 77 K was used to estimate the specific surface area (SSA) according to the Brunauer-Emmett-Teller (BET) method. The magnetic properties were measured using a Quantum Design 7 Tesla MPMS SQUID magnetometer.

3 RESULTS AND DISCUSSION

3.1 Crystallography, size, and morphology

The synthesised iron oxide nanoparticles were identified to be crystalline maghemite (γ-Fe_2O_3) from the X-ray diffraction (XRD) patterns (Figure 1). An amorphous–like peak broadening and overlapping between (220) and (311) peaks was observed at smaller crystallite size. This was possibly due to a certain degree of crystal disorder resulting from partial random distribution of cation vacancies in the cubic spinel structure of γ-Fe_2O_3 [2]. The size of the synthesized particles increased with higher liquid precursor feed flowrate (ml/min) to dispersion O_2 (L/min) ratio. At higher ratio, the flame enthalpy rate increased. Hotter flame, higher Fe-precursor concentration, and longer residence time resulted in the increase in coalescence and sintering of particles, and thus larger particle sizes [3].

TEM images of γ-Fe_2O_3 particles (Figure 2a-g) displayed more defined edges with increasing size, evolving from near-spherical to hexagonal and octagonal platelet shapes. Further investigation by tapping-mode AFM (Figure 3) was conducted to verify the shape of the largest particles (Figure 2g). The obtained average particle thickness of 4.5 nm based on 100 particle counts was smaller than the observed diameter of 57 nm from TEM for the same sample, confirming the platelet-like shape of the particles.

Different segregation of γ-Fe_2O_3 within the silica matrix at various Fe:Si ratio is distinctively evident from the TEM images of SiO_2/γ-Fe_2O_3 (Figure 2h-j). Single γ-Fe_2O_3 phase was visibly segregated to the edge of each silica particle at Fe:Si of 1:2, whereas a well-dispersed γ-Fe_2O_3 multi-cores embedded in spherical silica particles was observed at Fe:Si of 1:5. Similar conformation was noted by Ehrman et al. [4] for particles synthesised via a vapour-fed flame technique. Unlike bare γ-Fe_2O_3 particles, the γ-Fe_2O_3 cores did not assume the platelet shape in the presence of SiO_2, indicating that SiO_2 suppressed this morphological transformation [3].

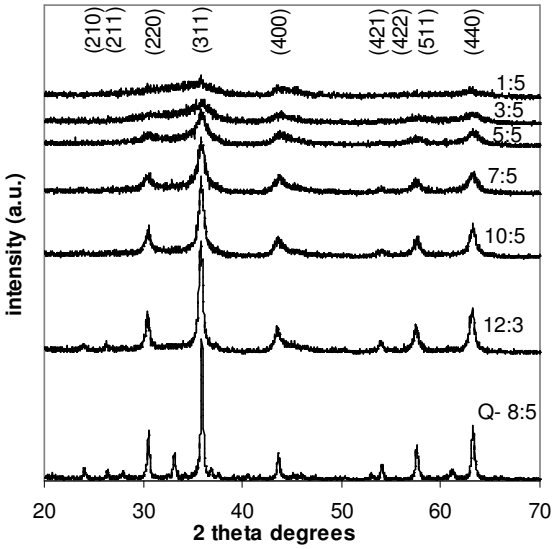

Figure 1: X-ray diffraction patterns of γ-Fe_2O_3 sprayed at various precursor flowrate to dispersion gas ratio (Q denotes the use of quartz tube)

The particle diameter of γ-Fe_2O_3 derived using the Scherrer formula for crystalline peak (311) (d_{XRD}) was quantitatively compared to those obtained by N_2 adsorption (d_{BET}) and from statistical counting of particle size from TEM images (d_{TEM}) (Figure 4). Good agreement was found for the smaller particles where the shapes were close to spherical with mono-crystalline structures. Larger deviation between d_{BET} and d_{TEM} in comparison to d_{XRD} was observed for particles formed in the flame encapsulated by quartz tube. The formation of twinned crystals for the particles as shown in Figure 2g could be the reason for smaller d_{XRD} observed here.

The particle size distribution obtained from statistical counting can be described by a log-normal distribution with a geometric standard deviation close to the theoretical self-preserving size distribution (SPSD) of 1.46 [5] for all sizes γ-Fe_2O_3 (Table 1). Decreasing geometric standard deviation with particle size was presumably due to less coalescence and sintering occurring at shorter residence time and lower flame temperature.

Incorporation of TEOS in the liquid precursor resulted in Bragg peaks at the same positions as those of pure γ-Fe_2O_3. This verifies that discrete γ-Fe_2O_3 and SiO_2 phases, rather than a single solid solution of the SiO_2/γ-Fe_2O_3

nanoparticles, were formed. An amorphous SiO_2 hump at 2θ = 20-40˚ was visible and became more pronounced at higher Si content (spectra not shown here). The γ-Fe_2O_3 core crystallite size (d_{XRD}) was found to decrease from 8 nm to 4 nm for Fe:Si = 1:2 to 1:5, respectively. In comparison to the obtained d_{TEM} of 19 nm and 11 nm, the discrepancy implies a possible presence of alternative Fe phase or a decrease in γ-Fe_2O_3 crystallinity.

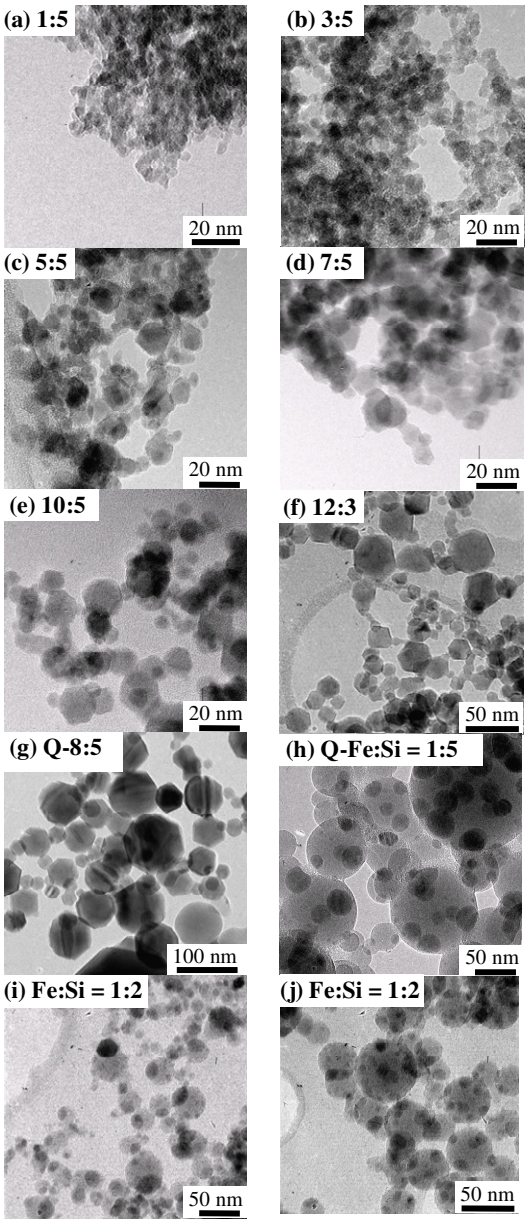

Figure 2: TEM micrographs of γ-Fe_2O_3 synthesised at various precursor flowrate to dispersion gas ratio, and SiO_2/γ-Fe_2O_3 nanoparticles at different Fe:Si ratio

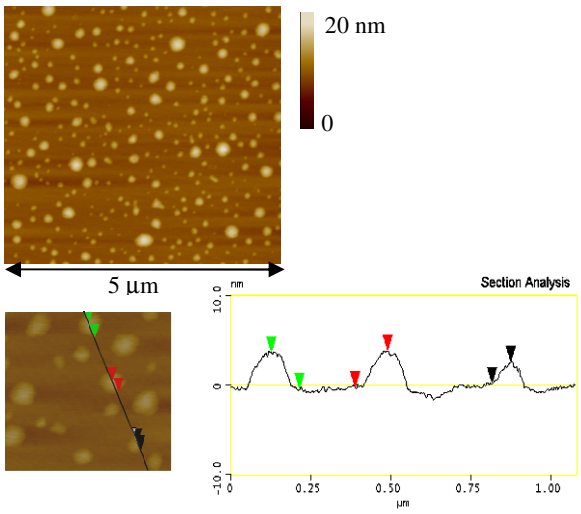

Figure 3: Image of AFM showing thickness of γ-Fe_2O_3 (Q-8:5, d_{TEM} = 57nm)

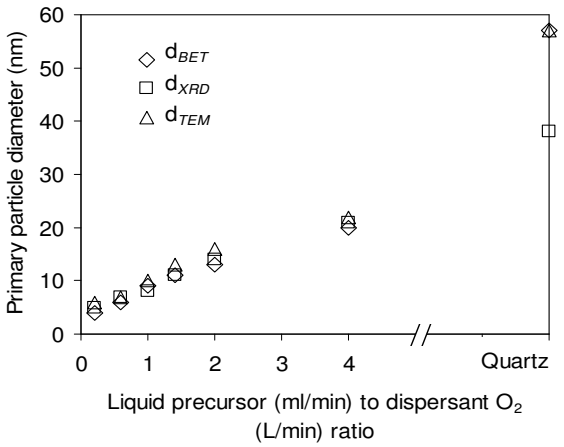

Figure 4: Comparison of γ-Fe_2O_3 particle diameter from various characterisation techniques

Table 1: Particle size distribution of γ-Fe_2O_3

Precursor/dispersion gas ratio	1/5	3/5	5/5	7/5	10/5	12/3
d_{TEM} (nm)	6	7	10	13	16	22
σ_g	1.36	1.36	1.39	1.42	1.42	1.52

3.2 Magnetic properties

All γ-Fe_2O_3 particles were found to be predominantly superparamagnetic at room temperature, with progressively greater proportion of ferromagnetic particles as the size increased. An almost linear dependency of saturation magnetisation (σ_s) and γ-Fe_2O_3 particle size (represented by d_{BET}) was observed (Figure 5), until the bulk σ_s of 74 emu/g is reached for d_{BET} > 13nm. Considerably lower σ_s at smaller sizes was likely due to surface-canting effect and

internal disorder of γ-Fe_2O_3 crystal [6]. The relatively drastic decrease in σ_s for 4nm particle could indicate a complete random cation vacancy distribution. An opposite trend of decreasing coercivity (H_c) at 5K with particle size was observed. The high coercivity values at small sizes also suggested additional anisotropies and structural disorder [6] supported by the somewhat amorphous-like XRD spectra.

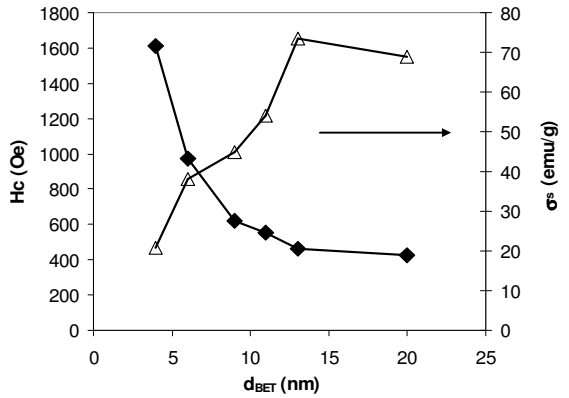

Figure 5: Correlation of saturation magnetism (σ_s) and coercivity (H_c) with γ-Fe_2O_3 particle size

A much lower overall magnetization than the bulk saturation value was measured for SiO_2/γ-Fe_2O_3 particles (Table 2). It is also interesting to note that the specific magnetization per unit mass of γ-Fe_2O_3 core in a silica matrix is lower compared to bare γ-Fe_2O_3 of similar d_{XRD} size. This is attributed to the presence of diamagnetic silica matrix, which inhibited the γ-Fe_2O_3 crystal growth. Inhibition of γ-Fe_2O_3 crystal growth in the presence of SiO_2 during FSP was confirmed by the decrease in geometric standard deviation reported in a previous study [3]. Tartaj et al [7] also concluded that the magnetic properties of SiO_2/γ-Fe_2O_3 composite are influenced by both the magnetic unit volume and the degree of dispersion of magnetic core within the matrix, since the inter-particle interactions could cause disturbance to the moments.

Table 2: Magnetic properties of SiO_2/γ-Fe_2O_3

Fe:Si	1:2	1:5	Q 1:5
Overall σ_s (emu/g)	12	6	12
Specific σ_s (emu/g of γ-Fe_2O_3)	38	40	57

4 CONCLUSIONS

One-step synthesis of γ-Fe_2O_3 and SiO_2/γ-Fe_2O_3 nanoparticles was carried out through flame spray pyrolysis. By balancing the inherent thermodynamics with controllable spraying conditions, the size and morphology of the nanoparticles can be tailored. Detailed examination of nanoparticles properties showed unique particle morphology transformation from near-spherical to hexagonal and octagonal platelet-shaped γ-Fe_2O_3 with increasing flame enthalpy rate. The decrease of σ_s with particle size was observed, attributed to a combinatorial effect of surface-canting and internal crystal disorder. In the case of SiO_2/γ-Fe_2O_3, varying Fe:Si ratio resulted in distinctively different γ-Fe_2O_3 core segregation inside a generally spherical silica matrix. The presence of SiO_2 was likely to suppress γ-Fe_2O_3 growth, subsequently leading to reduced core size variation and decreased specific magnetism.

ACKNOWLEDGMENTS

The authors thank Professor S. E. Pratsinis (ETH Zürich) and Dr. L. Mädler (UCLA) for FSP reactor design and setup; Professor Paul Munroe and Ms. Katie Levick (UNSW) for assistance with the TEM and AFM analysis. This work was carried out with the financial assistance of the Australian Research Council under the ARC Centres of Excellence Program.

REFERENCES

[1] Tartaj, P., Morales, M. P., Veintemillas-Verdaguer, S., Gonzales-Carreno, T., and Serna, C. J. 2006. Synthesis, properties, and biomedical applications of magnetic nanoparticles in Handbook of Magnetic Materials Buschow, K. H. J (ed).

[2] Morales, M. P.; Veintemillas-Verdaguer, S.; Montero, M. I.; Serna, C. J. *Chem. Mater.* **1999**, *11*, 3058.

[3] Li, D.; Teoh, W. Y.; Selomulya, C.; Woodward, R. C.; Amal, R.; Rosche, B. *Chem. Mater.* **2006**, *18*, 6403.

[4] Ehrman, S. H.; Friedlander, S. K. *J. Mater. Res.* **1999**, *14,* 4551.

[5] Pratsinis, S. E. *Prog. Energy Combust. Sci.* **1998**, *24,* 197.

[6] Morales, M. P.; Veintemillas-Verdaguer, S.; Serna, C. J. *J. Mater. Res.* **1999**, *14*, 3066.

[7] Tartaj, P.; González-Carreño, T; Serna, C. J. *J. Phys. Chem. B*. **2003**, *107*, 20.